Title

OsciDrop: A Versatile Deterministic Droplet Generator

Journal

Analytical Chemistry, 94(6)

ISSN

0003-2700

Authors

Ye, Shun
Li, Caiming
Zheng, Xu
et al.

Publication Date

2022-02-15

DOI

10.1021/acs.analchem.1c04852

pubs.acs.org/ac

analytical chemistry

February 15, 2022 Volume 94 Number 6

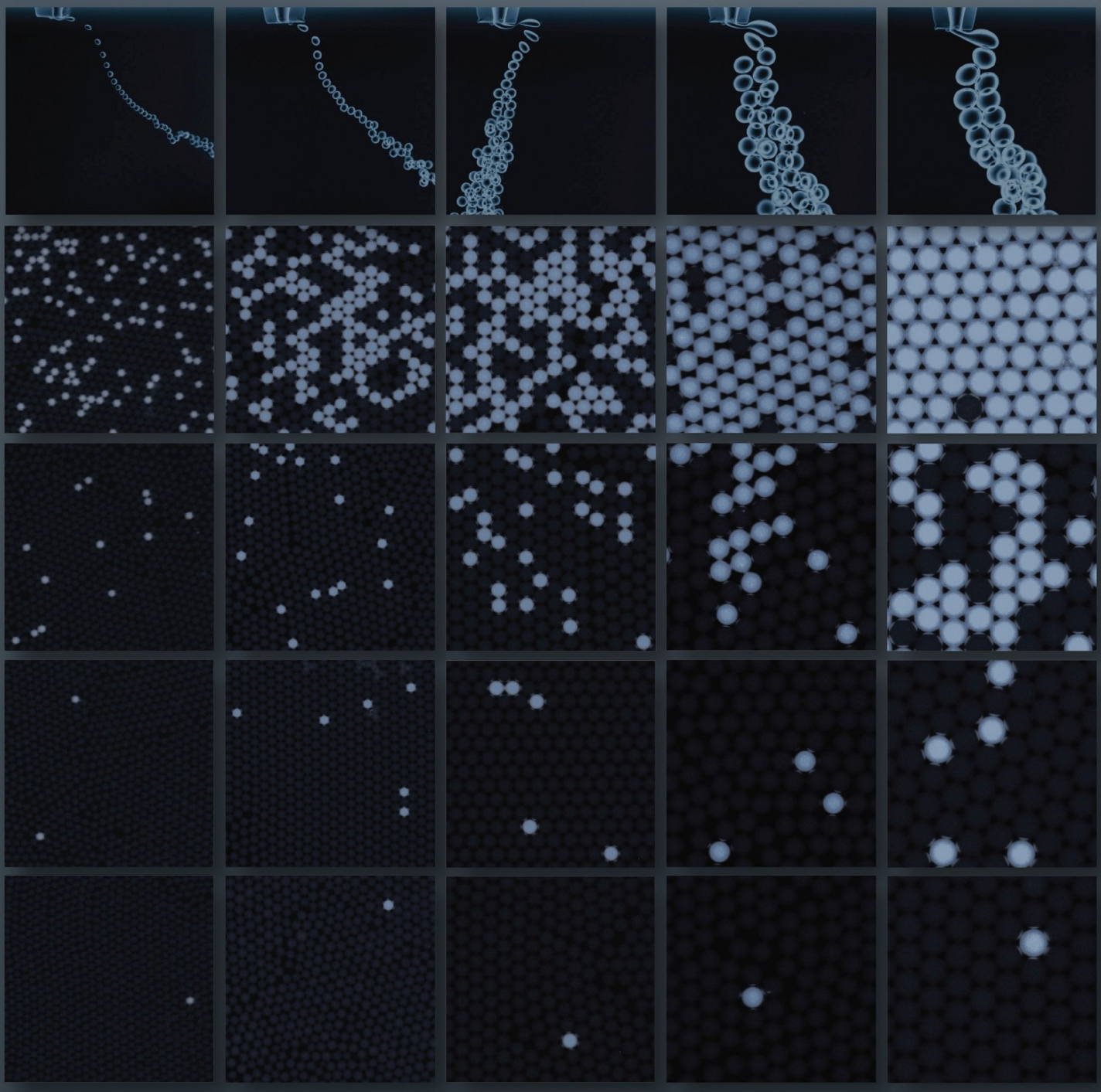

ACS Publications
Most Trusted. Most Cited. Most Read.

www.acs.org

analytical chemistry

pubs.acs.org/ac Article

OsciDrop: A Versatile Deterministic Droplet Generator

Shun Ye,[○] Caiming Li,[○] Xu Zheng,* Weihang Huang, Yi Tao, Yanghuan Yu, Limin Yang, Ying Lan, Liang Ma,* Shengtai Bian,* and Wenbin Du*

Cite This: *Anal. Chem.* 2022, 94, 2918−2925 Read Online

ACCESS | Metrics & More | Article Recommendations | Supporting Information

ABSTRACT: This paper describes OsciDrop, a versatile chip-free droplet generator used to produce size-tunable droplets on demand. Droplet generation is fundamental to miniaturized analysis. We designed OsciDrop to segment the fluid flowing out of the orifice of a disposable pipette tip into droplets by oscillating its distal end underneath an immiscible continuous phase. We described the theoretical model and investigated the effect of flow rate, oscillating amplitude, frequency, and waveform on droplet generation. Our study revealed a previously underexplored Weber number-dominated regime that leverages inertial force instead of viscous force to generate droplets. The same pipette tip allowed robust and deterministic generation of monodisperse droplets with programmable sizes ranging from 200 pL to 2 μL by asymmetrical oscillation. We validated this platform with two droplet-based nucleic acid amplification tests: a digital loop-mediated isothermal amplification assay for absolute quantification of African swine fever virus and a multi-volume digital polymerase chain reaction assay for the high dynamic range measurement of human genomic DNA. The OsciDrop method opens a facile avenue to miniaturization, integration, and automation, exhibiting full accessibility for digital molecular diagnostics.

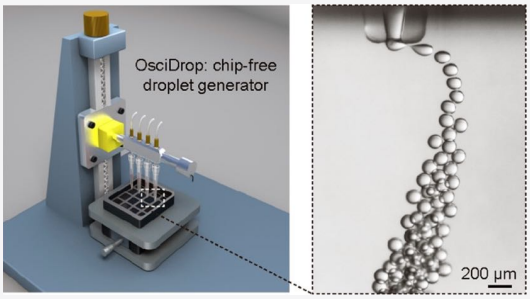

INTRODUCTION

The objective of this work was to design and characterize a chip-free droplet microfluidic method that allows deterministic droplet generation using low-cost pipette tips and demonstrate its application in digital nucleic acid amplification (dNAA). Droplet microfluidics is an attractive technology in many essential research areas such as biology, medicine, and chemistry due to inherent advantages such as ultra-high throughput, minimal consumption, and single-molecule/cell resolution.[1−3] Digital assays enable precise and absolute quantification of nucleic acids using end point analysis of amplification products inside compartments such as droplets. By performing the assay with multiple sets of droplet volumes, we can expand the detection range in a manageable and efficient way for nucleic acid quantification that is crucial for viral load analysis, bacterial detection, and precision oncology.[4,5] Microfabricated T-junction,[6,7] flow-focusing,[8] and step emulsification[9−11] designs are commonly used for viscous force-driven droplet generation. However, the size of droplets is limited to the microchannel geometry and varies with the flow rate, fluid viscosity, surface tension, and geometric imperfections in microchannels. Therefore, chip-based droplet microfluidics frequently demands meticulously formulated reagents, advanced fluidic control, and high-precision and costly microfabrication with specialized equipment.[12] These problems are exacerbated in the case of multi-volume digital assays, which further require complicated design and fabrication. In addition, the sophisticated chip configuration and operation often represent a significant technical barrier for inexperienced researchers and restrict their utility in both research and clinical settings.

Chip-free droplet generation methods bypass microfabrication, such as coflowing,[13] on-demand piezoelectric printing,[14−16] centrifugal emulsification,[17,18] and capillary/needle-based approaches,[19−23] and emerge as promising alternatives. For instance, we reported interfacial emulsification,[19] a simple method leveraging a capillary vibrating across the surface of the continuous phase for producing droplets with controllable volumes.[24−27] Similar approaches, such as spinning[20] or beveled[23] capillaries, have displayed substantial potential for widespread adoption due to reduced cost and simple instrumental settings. Nevertheless, these methods require manual pre-processing of the dispensing capillary, such as cutting, beveling, stretching, and connecting, which is not readily mass-manufacturable or user-friendly.

We describe the OsciDrop platform to overcome these challenges. OsciDrop is a versatile chip-free droplet generator that oscillates the distal ends of pipette tips in the continuous phase. The low-cost mass-manufacturable pipette tip is an ideal choice for consumables because it is well accepted in a laboratory setting and compatible with standardized multi-well

Received: November 9, 2021
Accepted: January 9, 2022
Published: January 21, 2022

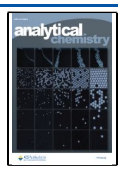

https://doi.org/10.1021/acs.analchem.1c04852
Anal. Chem. 2022, 94, 2918−2925

plates and automated liquid handling for ultimate scalability and throughput. Oscillation creates an inertial force that leads to deterministic and predictable monodisperse droplet generation with volume spanning picoliter to microliter spectrum tailored to specific needs such as multi-volume assays. Unlike conventional droplet microfluidic devices that rely on viscous force, working with well-controlled inertial force allows us to generate droplets of the same size with hydrocarbon oil and fluorinated oil with distinct viscosities and densities using the identical experimental setting. We depicted the physical principles of OsciDrop and quantitatively characterized the Weber number-dominated droplet generation mechanism. Based on this fundamentally new mechanism, we designed an asymmetrical waveform to ensure high robustness and tolerance to the geometric artifacts of the tip. With extremely low dead volumes, we can use OsciDrop to deliver a precise number of droplets in each well by specifying the injection volume. We adapted OsciDrop to perform two dNAA tests to demonstrate its feasibility and flexibility for molecular diagnostics with superior precision and dynamic range.

EXPERIMENTAL SECTION

Setup and Operation of OsciDrop. Custom-designed pipette tips (catalog no. con0001, Dawei Biotech, Beijing, China), 32-well plates with a flat bottom, the oscillating module, the syringe pumps, the displacement oil, and the droplet generation oil (catalog no. con0008, hydrocarbon-based) were obtained from Dawei Biotech. The OsciDrop platform consists of an in-parallel array of pipette tips attached to an oscillating module, a multi-well plate, and a high-precision vertical translation stage for locating the surface of droplet generation oil in the 32-well plate. The aqueous solution was aspirated into the pipette tips. The position of pipette tips was set to ∼0.3 mm under the air/oil interface over the multi-well plate filled with droplet generation oil. We used the OsciDrop platform to generate monodisperse droplets under the control of a computer program by adjusting the flow rate, oscillating amplitude, oscillating frequency, and waveform.

Digital Loop-Mediated Isothermal Amplification Assay. The digital loop-mediated isothermal amplification assay (dLAMP) assay kit for African swine fever virus (ASFV) consists of a set of primers, EvaGreen (Macklin, Shanghai, China), and LAMP reaction mix prepared as previously described.[25] The primers were designed using Primer Explorer 4 (https://primerexplorer.jp) (Table S1) and synthesized by InnoGen Biotech (Tianjin, China). First, the ASFV DNA stock solution was serially diluted with deionized (DI) water. Then, the ASFV DNA dilutions (4 μL) were added to the LAMP mix to a final reaction volume of 25 μL. Each reaction was converted into ∼18 400 1 nL droplets in four wells (4600 droplets in each microwell) on a 32-well plate by infusing at a flow rate of 120 nL/s and oscillating at 120 Hz. After applying the plate seal (Dawei Biotech), the dLAMP assay was performed at 66 °C for 60 min on a flat-block polymerase chain reaction (PCR) thermal cycler (Dawei Biotech).

Multi-volume Digital PCR. dPCR was performed in a 25 μL reaction, consisting of 12.5 μL of 2× dPCR Super Mix (Dawei Biotech), 6.9 μL of DI water, 0.6 μL of DNA polymerase (Dawei Biotech), 2.5 μL of 10× Primer&Probe, and 2.5 μL of template. We used a set of two primers and a probe synthesized by General Bio (Anhui, China) to quantify the EIF5B (Eukaryotic Translation Initiation Factor 5B) gene in human genomic DNA (gDNA) (Table S2). The standard gDNA (TaqMan Control Genomic DNA, Applied Biosystems, USA) was serially diluted in TE buffer to a concentration of 100 000, 10 000, 1000, 100, 10, and 1 copies/μL. The OsciDrop platform produced droplets of 0.2, 0.5, 1, 2.5, and 5 nL under 120 Hz with increased flow rates (from 24, 60, 120, 300, to 600 nL/s) to form planar monolayer droplet arrays (PMDAs) in 32-well plates (Table S3). We amplified the droplet arrays under the following PCR conditions on the flat-block PCR thermal cycler: 95 °C for 5 min, 45 cycles of 94 °C for 20 s and 58 °C for 1 min, and finally held at 25 °C.

Data Acquisition and Analysis. The pipette tips were imaged using an SMZ 800 stereoscope (Nikon, Japan) equipped with a Spot camera (SPOT Imaging, Sterling Heights, MI, USA). A cubic glass cell filled with droplet generation oil was used to capture high-speed microscopic imaging during droplet generation. We used an AcutEye high-speed camera (RockeTech, Changsha, Hunan, China) to record the droplet generation process. The droplet array was imaged using a Ti-E inverted microscope (Nikon, Tokyo, Japan) and a CoolSNAP HQ^2 camera (Photometrics, Tucson, AZ, USA). The quantities and diameters of droplets were obtained by analyzing the images using ImageJ software (NIH, Bethesda, MD, USA). The observed template concentrations of dLAMP and multi-volume digital PCR (MV-dPCR) were calculated based on Poisson distribution.[28]

RESULTS AND DISCUSSION

Origin and Verification of the OsciDrop Method. Micropipette tips are routinely used to transfer volumes of liquid in the microliter scale but not for nanoliter or picoliter droplets due to their large orifices (∼300−900 μm inner diameter, i.d.) and the limited precision of air displacement. To enable droplet generation, we designed the OsciDrop platform to dispense reagents under oscillation (Figure 1A). OsciDrop uses the positive displacement of the carrier oil to aspirate and dispense fluids with micropipette tips. We designed a plastic micropipette tip with a standard conical shape but a smaller orifice i.d. (120 μm), with a cost of less than $0.2 per tip. The key innovation is that OsciDrop leverages the forces created by moving the distal end of the micropipette tip under a stationary oil phase for droplet generation. Droplet volume could be tuned by adjusting parameters such as flow rate Q (nL/s), oscillating amplitude A (m), and oscillating frequency f (s^{-1}), as shown in Movie S1. The infusion rate of the dispersed aqueous phase is synchronized with the oscillation frequency to allow periodic droplet generation. During the continuous horizontal oscillation, the aqueous phase flowing out of the tip could be segmented into uniform-sized w/o droplets in sequence at high frequency through four parallel channels (Figure 1A,B). The symmetry of the oscillation waveform that dictates the force that particular size of droplets experience at different stages can be precisely engineered to achieve desired consistency and dynamic range of the droplet volume (Figure 1C,D).

To understand the physics of OsciDrop, we established a theoretical model based on the force balance (Figure 2A, see Text S1 for details). Before the droplet segmentation, the growing droplet lags behind the oscillating tip due to the viscous drag of the oil phase and forms a horizontal "neck" of the aqueous stream (Figure 2A). As a result, the droplet receives dynamic forces, including the interfacial tension F_σ, the viscous drag force F_v, the inertial force F_i, the gravity/buoyancy, the kinetic force, and the lift force. However, after theoretical calculations, only two major horizontal forces F_i and F_v are

https://doi.org/10.1021/acs.analchem.1c04852
Anal. Chem. 2022, 94, 2918−2925

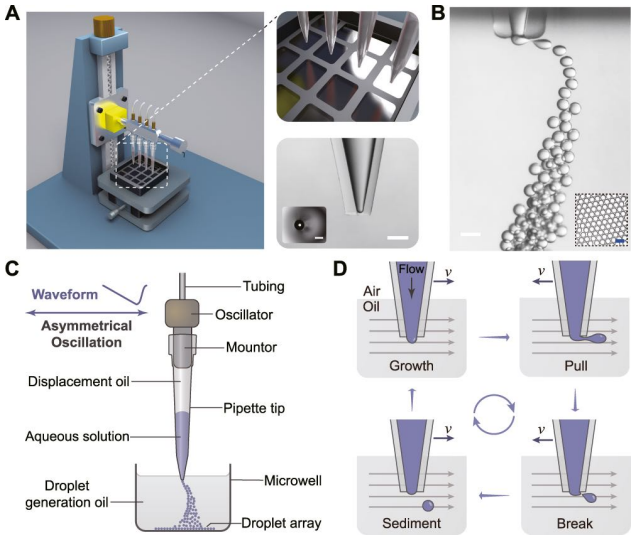

Figure 1. OsciDrop platform. (A) Schematic of the droplet generating platform consists of the oscillating module, a multi-well plate filled with droplet generation oil, and a vertical translation stage. The expended panel shows a magnified view of the pipette tips and the multi-well plate. Insets are the micrographs of the distal end of the pipette tip. The scale bar is 400 μm. (B) Microscopic images of generating water-in-oil (w/o) droplets in a cubic glass cell and the PMDA at the flat bottom of the microwell (shown in inset). The scale bar is 200 μm. (C) Schematic of an oscillating pipette tip with its orifice underneath the oil to segment the aqueous solution into monodisperse droplets. (D) Schematics showing the droplet generation cycle. The gray arrows indicate the direction of relative motion of the oil phase.

considered to balance the F_σ, which resists the neck break-off; other forces are neglected to simplify the theoretical model as follows

$$F_i + F_v = F_\sigma \tag{1}$$

The forces on the left-hand side of eq 1 try to detach the droplet from the aqueous stream, while the interfacial tension on the right-hand side resists the neck break-off. A successful droplet segmentation occurs when the summation of F_i and F_v exceeds F_σ.

Based on our theoretical evaluation, we set up the OsciDrop platform. We tested the droplet generation using various oscillation waveforms such as sine, square, and triangle waves (see Text S1 and Figure S1 for details). The initial results showed that it was technically challenging to generate monodisperse droplets in a controllable fashion using symmetrical oscillations because the summation of F_i and F_v may exceed F_σ twice during each oscillation cycle (Text S1). Therefore, we hypothesized that an asymmetrical oscillation waveform consisting of a long smooth stage with minimal perturbation for droplet growth and a short high-momentum segmenting stage would reliably generate monodisperse droplets. Thus, we designed an asymmetrical waveform (Figure S2) containing a long triangle wave and a short cosinusoidal wave. We successfully produced monodisperse 1 nL droplets with OsciDrop by asymmetrical oscillation (A = 0.55 mm and f = 120 Hz) at a flow rate of 120 nL/s. As shown in Figure 2B, the aqueous stream bulged and elongated during the long initial growth stage. The head of the stream was segmented into a droplet during the short segmenting stage, which establishes the feasibility for the OsciDrop concept.

Mechanism and Control Parameters of OsciDrop. To quantitatively describe the droplet generation process, we define the flow rate within a single oscillating circle as Q_c, which is specified as

$$Q_c = \frac{Q}{f} \tag{2}$$

where Q (nL/s) and f (s^{-1}) are the flow rate and oscillating frequency, respectively. The droplet generation frequency could be the same as the oscillating frequency, resulting in a produced droplet volume V (nL) equal to Q_c (nL) under suitable conditions. To validate the effectiveness of the asymmetrical oscillation, we generated droplets at a fixed flow rate of 240 nL/s with OsciDrop using increasing oscillating frequencies (i.e., 40, 80, 120, 160, and 200 Hz; Figure 2C and Movie S2). We measured the generated droplet volumes by analyzing the images of PMDAs and plotted the results in Figure 2D. According to eq 2, higher oscillating frequencies generated smaller droplets with a fixed Q due to decreased Q_c values. We found that the experimental results of droplet volumes matched very well with the theoretical calculations. Thus, it is intuitive to predict and control droplet volumes by OsciDrop.

To find out the primary control parameters of OsciDrop, we further analyzed the force balance mentioned above and deduced the following equation

$$We\frac{u_f}{u}R + 6Ca\left(1 - \frac{u_f}{u}\right)R = d_{neck} \tag{3}$$

Here, We refer to the Weber number, defined as $We = \rho R_{tube}^2 uTa/\sigma R$, which represents the ratio between the inertial force and the interfacial tension, Ca refers to the capillary number, defined as $Ca = \eta u/\sigma$, which is the ratio between the viscous force and the interfacial tension, and d_{neck} (m) is the characteristic dimension of the neck region. Here, R_{tube} (m) is the tube radius in the tip, ρ (kg/m^3) is the density of the aqueous phase, σ (N/m) is the surface tension at the aqueous/oil interface, η (kg/m·s) is the dynamic viscosity of oil, T (s) is the period of oscillation, and a (m/s^2) is the acceleration of the oscillation.

Equation 3 describes the relation among the We number, Ca number, aqueous phase injection speed u_f (m/s), the oscillating speed u (m/s), and the generated droplet radius R (m). Our calculation shows that the We number ($We \sim 20-40$) is much larger than the Ca number ($Ca \sim 0.05-0.5$), indicating a We-dominated droplet segmentation mechanism (see Text. S1.4 for details). In other words, the inertial force F_i is the dominant force that determines droplet segmentation. For the asymmetrical oscillation combining triangle wave and cosinusoidal wave, we obtained the temporal variations of F_i

$$F_i = \begin{cases} 0 & \left(0 < t < \frac{4}{5}T\right) \\ QAf^2\rho t(5\pi)^2\cos\left[\frac{5\pi}{T}\left(t - \frac{4}{5}T\right)\right] & \left(\frac{4}{5}T < t < T\right) \end{cases} \tag{4}$$

where t (s) is the elapsed time within an oscillation period. According to eqs 1 and 4, during the initial stage, the head of the aqueous stream bulges and elongates in the oil phase since F_v could hardly exceed the F_σ without the F_i; during the segmenting stage, the droplet detaches due to the dramatically increased F_i, and F_i is positively proportional to Q, A, and f^2.

https://doi.org/10.1021/acs.analchem.1c04852
Anal. Chem. 2022, 94, 2918−2925

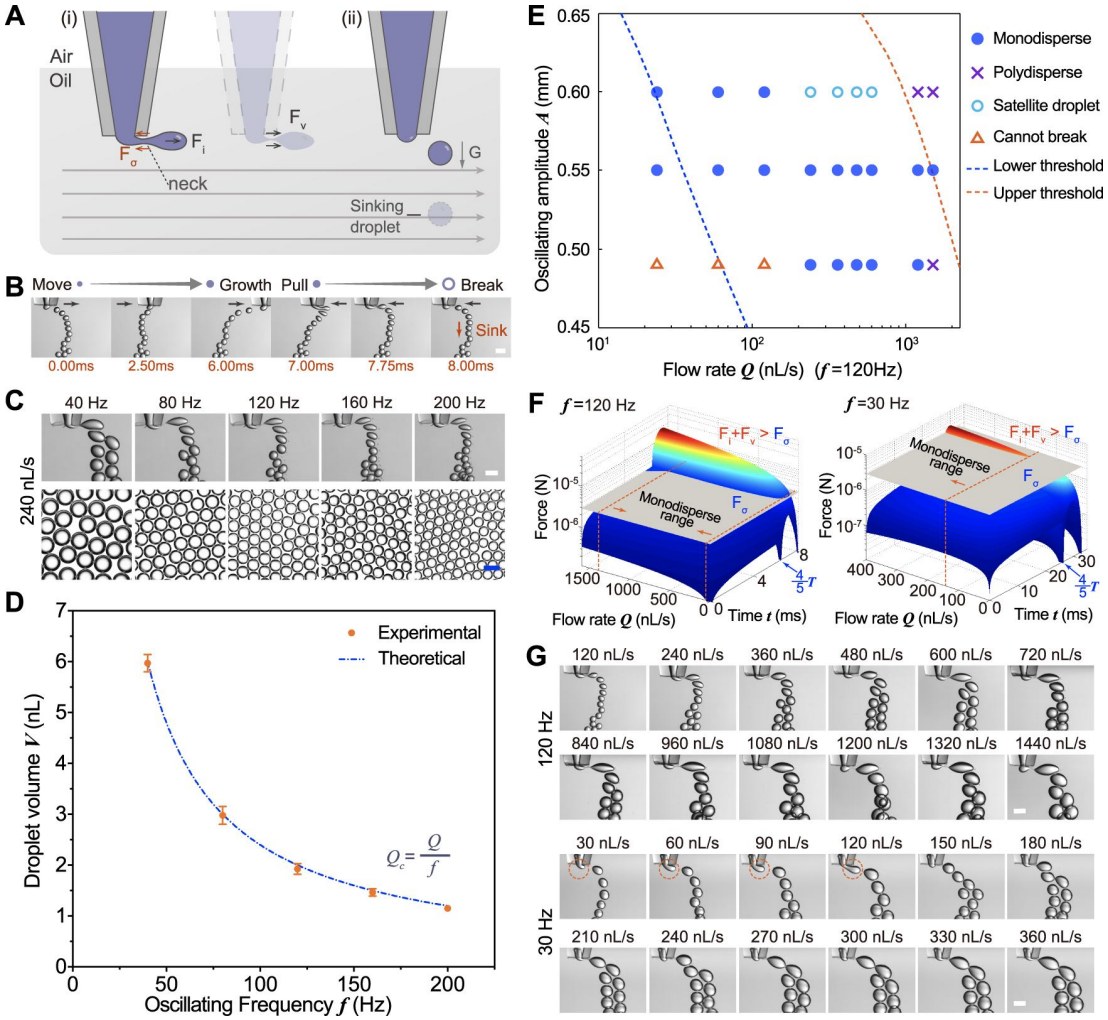

Figure 2. Physical phenomenon of OsciDrop. (A) Force analysis of droplet segmentation by a pipette tip. Gray arrows indicate the direction of relative motion of the oil phase. (B) Time series microscopic images of the droplet generation by OsciDrop, including an initial growth stage and a segmenting stage. Black arrows indicate the moving direction of the pipette tip. (C) Images of droplet segmentation by OsciDrop under frequencies f from 40 to 200 Hz at a fixed flow rate Q of 240 nL/s and the generated droplets. (D) Droplet volume V at different frequencies f when Q = 240 nL/s. The blue dashed line represents the theoretical calculation. (E) Phase diagram for droplet generation by OsciDrop showing the region of deterministic segmentation (f = 120 Hz). Blue dots represent experiments with deterministic segmentation, and dashed lines represent theoretical lower and upper thresholds. (F) Three-dimensional plots showing the temporal variations of $F_i + F_v$ (colored curved surface) and F_σ (gray surface) during one period T (f = 120 and 30 Hz). We achieved a deterministic droplet segmentation when the summation of F_i and F_v exceeds F_σ during segmenting stage (4/5 T to T). (G) Images of droplet segmentation under increasing Q_c (Q/f) from 1 to 12 nL at f of 120 Hz and 30 Hz. The orange dashed circles indicate that a droplet segmentation needs multiple oscillation cycles when Q_c is below the threshold. Scale bars are 200 μm.

Based on eq 4, we find that under a fixed f, decreasing A decreases the inertial force F_i during the segmenting stage, which could lead to ineffective droplet segmentation for generating tiny droplets. On the other hand, a too-large A leads to a large inertial force F_i that may produce either satellite droplets or poor monodispersity at high flow rates. Thus, we hypothesize that a suitable range of A exists to generate monodisperse droplets. We tested this hypothesis by varying A (i.e., ~0.5, 0.55, and 0.60 mm) with flow rate Q ranging from 24 to 1320 nL/s, and f was set as 120 Hz. Experimental results (symbols) and theoretical prediction (dashed lines) are summarized in Figure 2E: the orange triangles show that the aqueous stream cannot be segmented into droplets during one oscillating circle at low flow rates, the cyan open circles indicate satellite droplet generation, and the purple checkmarks represent high polydispersity (volume coefficient of variation (CV) > 10%). We found that 0.55 mm is the most suitable A under such tested conditions, generating monodisperse droplets (volume CV ≤ 10%, shown as blue dots in Figure 2E) spanning a wide range of flow rates. We produced droplets from 200 pL to 12 nL by simply changing the flow rate with a fixed oscillation condition (A = 0.55 mm and f = 120 Hz).

In addition to the oscillating amplitude, the oscillating frequency f also plays an important role in determining droplet segmentation. Theoretically, the reduced f leads to dramatically decreased F_i that is inadequate to generate tiny droplets. We calculated the temporal variations of $F_i + F_v$ and F_σ to predict the droplet segmentation and delimit different working ranges (Text S1). The forces at 120 and 30 Hz asymmetrical oscillations during one period T are compared in Figure 2F. According to our theoretical prediction, the summation of F_i and F_v (shown as colorful curved surface) dramatically reduces in response to decreased frequency, especially during the segmenting stage,

https://doi.org/10.1021/acs.analchem.1c04852
Anal. Chem. 2022, 94, 2918−2925

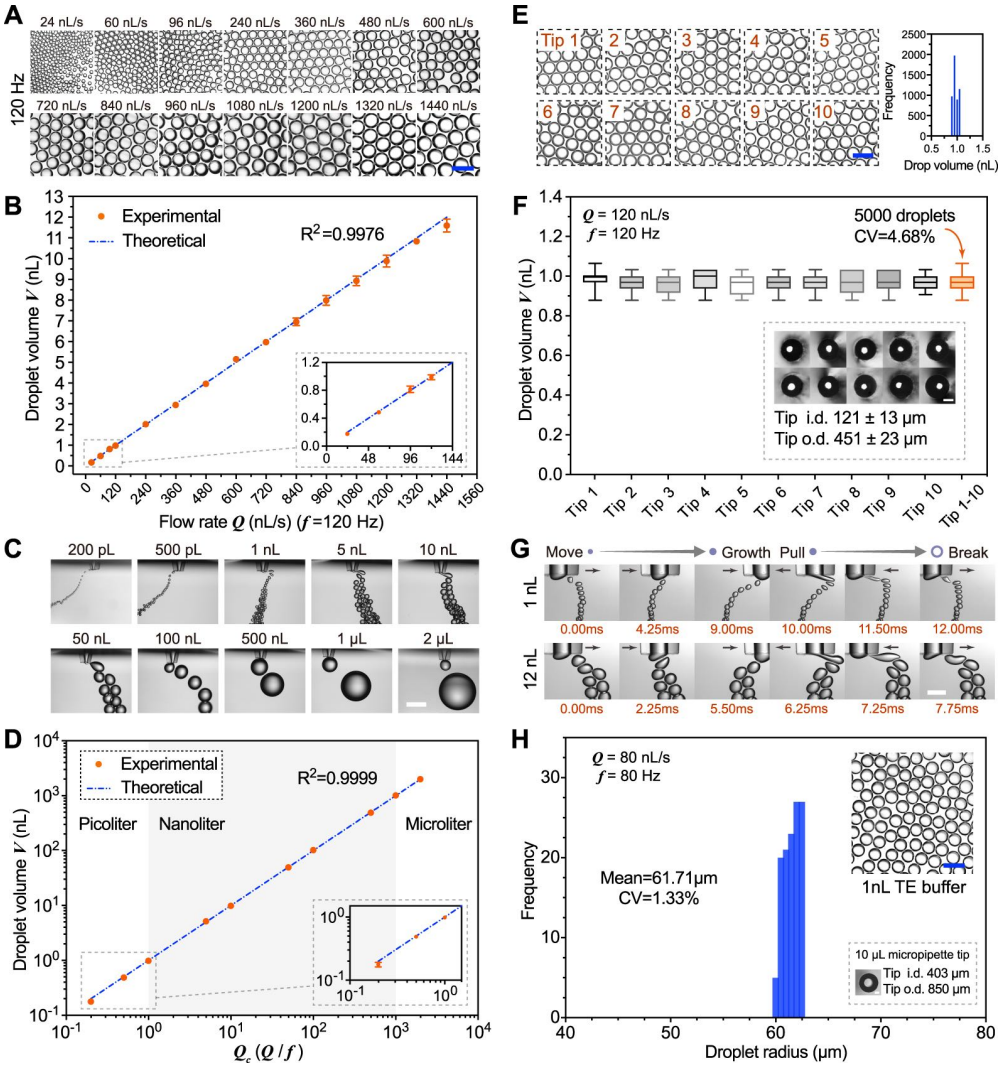

Figure 3. Deterministic droplet generation with OsciDrop. (A) At an amplitude A of 0.55 mm under the 120 Hz oscillation, the droplet sizes increase monotonically with the flow rate Q (24−1440 nL/s). The scale bar is 400 μm. (B) Linear correlation between the droplet volume V and the flow rate Q at 120 Hz. (C) Size-tunable droplet generation by simultaneously adjusting Q, A, and f. The scale bar is 800 μm. (D) Linear correlation between the droplet volume V and the calculated Q_c. (E) High consistency of randomly picked pipette tips in droplet generation. All generated droplets are highly monodisperse with an accurate droplet volume of 1 nL. (F) Volume distribution of droplets generated using Tip 1 to Tip 10 (with orifices shown in inset), with an aggregated CV of 4.68% (n = 5000). (G) Time series imaging of the droplet generation with expected volumes of 1 and 12 nL using a standard 10 μL pipette tip. Black arrows indicate the moving direction of the pipette tips. The scale bar is 400 μm. (H) Radius distribution of 1 nL droplets generated using a standard 10 μL pipette tip (shown in the inset). Scale bars are 200 μm (E, F, and H).

resulting in ineffective droplet segmentation under small Q_c values.

To verify our theoretical evaluation based on eqs 3 and 4, we tested droplet generation by varying Q_c from 1 to 12 nL with A = 0.55 mm under 120 and 30 Hz oscillations, respectively (Figure 2G). The results show that we can generate monodisperse droplets with all Q_c values tested under the 120 Hz oscillation. In contrast, it cannot segment the aqueous stream within a single oscillation period when $Q_c \leq 4$ nL under the 30 Hz oscillation. The monodisperse ranges under two different oscillating frequencies matched very well with the theoretical prediction. These results thus provide a guide for robust droplet generation using OsciDrop.

Deterministic Droplet Generation Using OsciDrop. We then examined the predictability and flexibility of OsciDrop for generating monodisperse droplets. First, keeping the oscillating amplitude constant at 0.55 mm under 120 Hz oscillation as described above, we observed that the droplet size increased monotonically and scales linearly (R^2 = 0.9976) with flow rate Q from 24 to 1440 nL/s as predicted (Figure 3A,B). Then, we also measured the generated droplet volume V and plotted the results in Figure 3B. Thus, it provides an intuitive way to adjust droplet volumes (200 pL to 12 nL) by simply changing the flow rates within this monodisperse range.

Although we can quickly achieve size-tunable droplet generation by adjusting flow rates, it is technically challenging to produce monodisperse droplets spanning a broad volume range (e.g., from picoliter to microliter range) with fixed oscillating amplitude and frequency. Therefore, we next investigated the flexibility of OsciDrop for generating droplets from picoliter to microliter scale that is conventionally difficult to achieve in either chip-based or chip-free methods. By adjusting three primary control parameters simultaneously, including Q, A, and f (Table S4), we successfully generated

https://doi.org/10.1021/acs.analchem.1c04852
Anal. Chem. 2022, 94, 2918−2925

monodisperse droplets spanning 200 pL to 2 μL range, as shown in Figure 3C and Movie S3. The linear correlation between the generated droplet volumes V and calculated Q_c value matched well with theoretical calculations (R^2 = 0.9999, Figure 3D), validating the flexible droplet generation with tunable volumes spanning 5 orders of magnitude.

Robustness Evaluation of OsciDrop. In contrast to high-precision photolithography and microfabrication processes, plastic pipette tips fabricated by conventional injection molding exhibit higher variations in the inner/outer diameters (i.d./o.d.) and molding flashes. To evaluate the tolerance of OsciDrop to geometric artifacts induced by fabrication, we generated droplets with an expected volume of 1 nL using 10 randomly picked pipette tips. The generated PMDAs were then recorded and quantitatively analyzed (Figure 3E). At a flow rate of 120 nL/s and an oscillating frequency of 120 Hz, 5000 droplets of 1 nL volume were generated by 10 pipette tips with a CV of 4.68%. Figure 3E,F plots the volume distribution of droplets produced by Tip 1 to Tip 10 (shown in inset; i.d. 121 ± 13 μm, o.d. 451 ± 23 μm; mean ± SD). This feature demonstrates OsciDrop's considerable potential in applications where generating droplets with precise volumes are required.

Although the above results reflect the excellent robustness of OsciDrop, the customized pipette tips having a smaller i.d. are not readily accessible in many laboratories, which may represent a practical barrier for adopting OsciDrop. Therefore, we examined the feasibility of generating droplets using standard pipette tips available in most biomedical laboratories. As a result, we produced droplets with expected volumes of 1 and 12 nL using standard 10 μL pipette tips (i.d. 403 μm and o.d. 850 μm) by tuning three control parameters as shown in Figure 3G. The radius distribution of 1 nL droplets generated at the flow rate of 80 nL/s under the 80 Hz asymmetrical oscillation is highly uniform with a volume CV of 1.33% (Figure 3H, see Text S2 and Figure S3 for details).

Further improvement in OsciDrop's performance could be made by fine-tuning control parameters, optimizing oscillation waveforms, and using high-precision syringe pumps (see Texts S3 and S4 and Figures S4-S7). We also validated that OsciDrop can generate nanoliter droplets using a commercially available fluorinated oil of very different viscosity and density than hydrocarbon-based droplet generation oil (Text S3 and Figures S6 and S7), owing to the *We*-dominated mechanism that is not sensitive to oil viscosity and density. Distinct from the existing droplet generators on the market, OsciDrop allows accurate and flexible control of droplet volumes without redesigning microfluidics chips. This feature allows flexibility in experimental design and improves efficiency at a reduced cost for assay developers.

Quantification of ASFV by dLAMP. Having shown the capability of OsciDrop to generate monodisperse droplets, we validated its functionality with dNAA tests. The recent spread of ASFV has caused severe animal pandemics and economic losses to the global swine industry.[29] To allow rapid and high sensitive detection of ASFV, we designed and performed a dLAMP assay for absolute quantification of the ASFV as schematically illustrated in Figure 4A. The OsciDrop platform utilized four parallel channels to generate monodisperse droplets encapsulating nanoliter LAMP reactions. To test the linearity of the assay, we serially diluted ASFV DNA stock solution by 1×, 4×, 30×, and 100× folds and performed droplet generation and dLAMP assay in 32-well plates. Figure 4B shows the end point fluorescent images of dLAMP reaction solutions with different

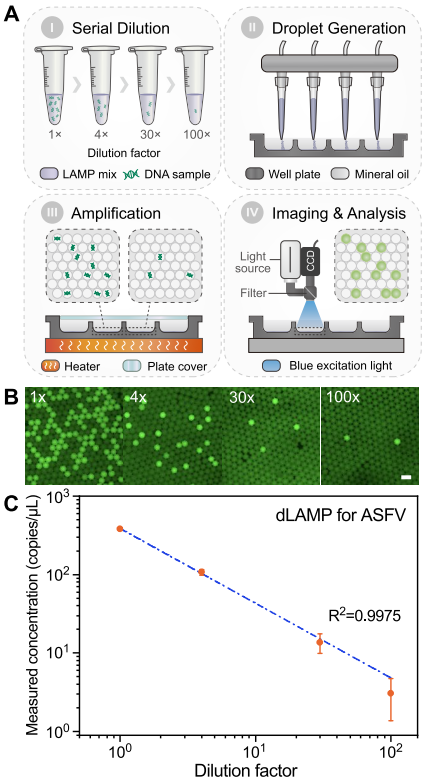

Figure 4. dLAMP of the African swine fever virus. (A) dLAMP workflow includes serial dilution of the ASFV DNA stock solution, four-channel droplet generation for sample segmentation, isothermal amplification, and fluorescence detection and quantitative analysis. (B) End point fluorescent images of PMDAs in dLAMP assays of serial dilutions (1×, 4×, 30×, and 100×) of the ASFV samples. (C) Linear correlation (blue dashed line) between the measured concentration and the dilution factor of the DNA samples.

dilution factors. Positive droplets containing amplified templates displayed strong fluorescence signals that are 3-fold higher than that of negative droplets. Furthermore, the measured concentrations were linearly correlated with the dilution factor with an R^2 of 0.9975 (Figure 4C). We obtained a lower detection limit of ~3 copies/μL when the partition volume was set to 1 nL, demonstrating the compatibility of OsciDrop with highly sensitive dLAMP tests.

MV-dPCR Quantification of Human gDNA. Next, we evaluated the utility of OsciDrop's capability to generate droplets with multiple predefined volumes in molecular tests. The standard dPCR suffers from a narrow dynamic range and trade-off between sensitivity and limit of quantification due to a fixed partition volume. Thus, an MV-dPCR harnessing OsciDrop's flexibility of on-demand droplet generation would further increase both the precision and dynamic range (Figure 5A). We evaluated OsciDrop's performance in MV-dPCR by quantifying the EIF5B reference gene in a set of serially diluted samples of human gDNA. We tested partition volumes of 0.2, 0.5, 1, 2.5, and 5 nL. As shown in Figure 5B, the fractions of positive droplets increased with larger partition volumes at the same concentrations. At the high concentration of 10^4 copies/μL, the fractions of positive droplets reached saturation at large partition volumes such as 2.5 and 5 nL, leading to unquantifiable template concentrations. Afterward, we plotted the fractions of positive droplets with input gDNA copies for each partition volume based on theoretical calculations (Figure S8A). Results

https://doi.org/10.1021/acs.analchem.1c04852
Anal. Chem. 2022, 94, 2918−2925

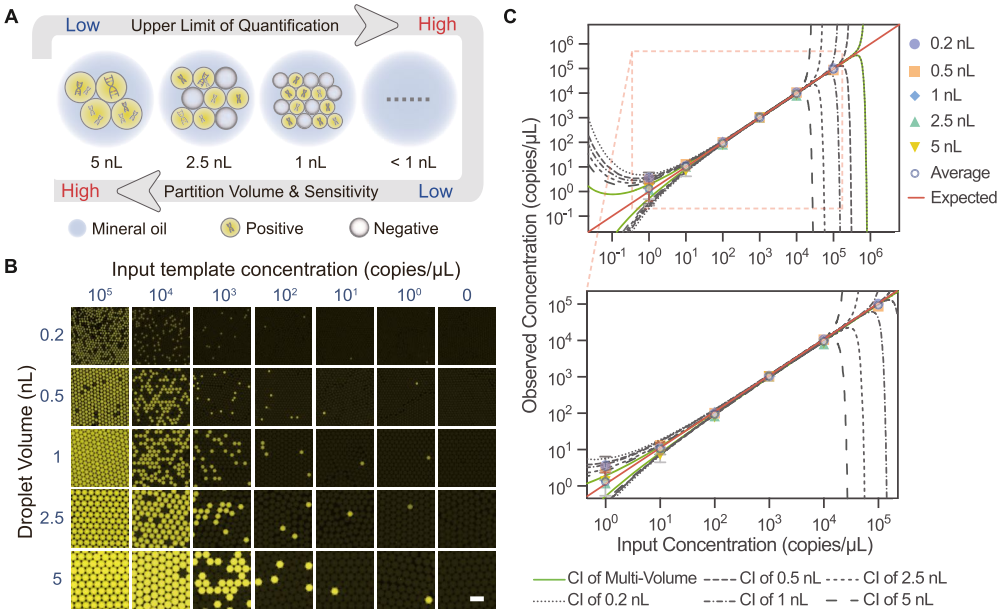

Figure 5. MV-dPCR using OsciDrop. (A) Schematic shows the principle of MV-dPCR using different droplet volumes to expand the dynamic range of quantification. (B) End point results for MV-dPCR using human gDNA with OsciDrop. Generally, the fraction of positive droplets increase with increasing partition volumes (i.e., 0.2, 0.5, 1, 2.5, and 5 nL). The fraction of positive droplets became 1 for large partition volume (e.g., 1, 2.5, and 5 nL) when the input gDNA template concentration is 100 000 copies/μL. The scale bar is 200 μm. (C) Comparison of input gDNA template concentrations and MV-dPCR observed concentrations over a dynamic range spanning 6 orders of magnitude.

showed that when partition volumes were 2.5 or 5 nL, the upper limits of quantification were far lower than that of 0.2 or 0.5 nL. We also calculated the 95% confidence interval (CI) for different partition volumes based on Majumdar et al.'s model.[30] We found that the width of CI for large partitions of 2.5 and 5 nL increased rapidly when the fractions of positive droplets were lower than 0.2, indicating suboptimal accuracy (Figure S8B and Table S5). Next, we examined the linearity of observed concentrations for serial dilutions of gDNA samples using the multi-volume approach (Figure 5C). We compared the 95% CI for each partition volume with theoretical calculations using Kreutz et al.'s multi-volume model.[28] The experimental results closely matched the theoretical predictions, indicating that the OsciDrop-based platform can readily implement MV-dPCR assays with a wide dynamic range over 6 orders of magnitude.

CONCLUSIONS

This paper established OsciDrop, a robust and versatile droplet generating method, using disposable pipette tips to achieve deterministic droplet segmentation under asymmetrical oscillation. The OsciDrop method depicts a unique *We*-dominated droplet generation mechanism utilizing the inertial force from the asymmetric oscillation, different from conventional droplet microfluidics that commonly works in a *Ca*-dominated regime. Furthermore, we demonstrated the feasibility of size-tunable generation of pico-/nano-/microliter droplets with high uniformity by adjusting the flow rate, oscillating amplitude, and frequency. Several vital advantages of OsciDrop, such as predictability, repeatability, robustness, and high dynamic range, were also verified by dLAMP and MV-dPCR assays. Notably, the pipette tips can be mass-manufactured at low cost with injection molding technique and allow complete automation of the liquid handling and droplet generation process. Furthermore, we envision that we can readily develop an 8-channel or a 96-channel module to increase the sample throughput, allowing plate-to-plate and sample-to-droplet conversion of 8 or 96 samples in parallel in a single step. Overall, deterministic droplet generation makes OsciDrop highly attractive for numerous applications in miniaturized analysis, making it well suited to advancing quantitative bioanalyses for molecular diagnostics and global health.

ASSOCIATED CONTENT

Supporting Information

The Supporting Information is available free of charge at https://pubs.acs.org/doi/10.1021/acs.analchem.1c04852.

Detailed version of theoretical analysis of droplet segmentation by OsciDrop; droplet generation using the standard 10 μL pipette tip; LAMP primers used in ASFV detection; validated parameters for generating monodisperse droplets using OsciDrop; and graphical summary of the MV-dPCR quantification range and precision (PDF)

Droplet generation by OsciDrop (AVI)

Droplet generation under increasing oscillating frequencies (AVI)

Size-tunable generation of droplets from 200 pL to 2 μL (AVI)

Droplet generation using fluorinated oil as continuous phase (AVI)

AUTHOR INFORMATION

Corresponding Authors

Xu Zheng − *State Key Laboratory of Nonlinear Mechanics, Institute of Mechanics, Chinese Academy of Sciences, Beijing 100190, China;* orcid.org/0000-0002-2398-9283; Email: zhengxu@lnm.imech.ac.cn

Liang Ma − *Dawei Biotechnologies Co., Ltd., Beijing 100085, China;* Email: liangma.chem@gmail.com

https://doi.org/10.1021/acs.analchem.1c04852
Anal. Chem. 2022, 94, 2918−2925

Shengtai Bian − *School of Sport Science, Beijing Sport University, Beijing 100084, China*; Email: stbian@bsu.edu.cn

Wenbin Du − *State Key Laboratory of Microbial Resources, Institute of Microbiology, Chinese Academy of Sciences, Beijing 100101, China; Savaid Medical School and College of Life Sciences, University of the Chinese Academy of Sciences, Beijing 100049, China;* orcid.org/0000-0002-7401-1410; Email: wenbin@im.ac.cn

Authors

Shun Ye − *State Key Laboratory of Microbial Resources, Institute of Microbiology, Chinese Academy of Sciences, Beijing 100101, China;* Present Address: Present address: Biomedical Engineering Department, College of Engineering, Pennsylvania State University, University Park, PA 16802, USA; orcid.org/0000-0003-3457-9359

Caiming Li − *State Key Laboratory of Microbial Resources, Institute of Microbiology, Chinese Academy of Sciences, Beijing 100101, China; College of Life Sciences, University of the Chinese Academy of Sciences, Beijing 100049, China*

Weihang Huang − *Department of Linguistics and Modern Languages, The Chinese University of Hong Kong, Hong Kong SAR 999077, China*

Yi Tao − *State Key Laboratory of Microbial Resources, Institute of Microbiology, Chinese Academy of Sciences, Beijing 100101, China*

Yanghuan Yu − *State Key Laboratory of Microbial Resources, Institute of Microbiology, Chinese Academy of Sciences, Beijing 100101, China*

Limin Yang − *CAS Key Laboratory of Pathogenic Microbiology and Immunology, Institute of Microbiology, Chinese Academy of Sciences, Beijing 100101, China*

Ying Lan − *State Key Laboratory of Microbial Resources, Institute of Microbiology, Chinese Academy of Sciences, Beijing 100101, China*

Complete contact information is available at: https://pubs.acs.org/10.1021/acs.analchem.1c04852

Author Contributions

○S.Y. and C.L. contributed equally to this work.

Notes

The authors declare no competing financial interest.

■ ACKNOWLEDGMENTS

This work was supported by the National Key Research and Development Program of China (2021YFC2301000, 2021YFA0717000, 2018YFC0310703, and 2016YFE0205800), the National Natural Science Foundation of China (21822408, 91951103, 12072350, and 11832017), and the CAS Strategic Priority Research Program (XDB22040403). We thank anonymous reviewers for suggestions to test the compatibility of OsciDrop with fluorinated oil.

■ REFERENCES

(1) Pompano, R. R.; Liu, W.; Du, W.; Ismagilov, R. F. *Annu. Rev. Anal. Chem.* **2011**, *4*, 59−81.
(2) Mashaghi, S.; Abbaspourrad, A.; Weitz, D. A.; van Oijen, A. M. *TrAC, Trends Anal. Chem.* **2016**, *82*, 118−125.
(3) Hu, B.; Xu, P.; Ma, L.; Chen, D.; Wang, J.; Dai, X.; Huang, L.; Du, W. *Mar. Life Sci. Technol.* **2021**, *3*, 169−188.
(4) Yen, G. S.; Fujimoto, B. S.; Schneider, T.; Kreutz, J. E.; Chiu, D. T. *J. Am. Chem. Soc.* **2019**, *141*, 1515−1525.
(5) Shen, F.; Sun, B.; Kreutz, J. E.; Davydova, E. K.; Du, W.; Reddy, P. L.; Joseph, L. J.; Ismagilov, R. F. *J. Am. Chem. Soc.* **2011**, *133*, 17705−17712.
(6) Thorsen, T.; Roberts, R. W.; Arnold, F. H.; Quake, S. R. *Phys. Rev. Lett.* **2001**, *86*, 4163−4166.
(7) Nisisako, T.; Torii, T.; Higuchi, T. *Lab Chip* **2002**, *2*, 24−26.
(8) Anna, S. L.; Bontoux, N.; Stone, H. A. *Appl. Phys. Lett.* **2003**, *82*, 364−366.
(9) Sugiura, S.; Nakajima, M.; Iwamoto, S.; Seki, M. *Langmuir* **2001**, *17*, 5562−5566.
(10) Stolovicki, E.; Ziblat, R.; Weitz, D. A. *Lab Chip* **2017**, *18*, 132−138.
(11) Nie, M.; Zheng, M.; Li, C.; Shen, F.; Liu, M.; Luo, H.; Song, X.; Lan, Y.; Pan, J.-Z.; Du, W. *Anal. Chem.* **2019**, *91*, 1779−1784.
(12) Whitesides, G. M.; Ostuni, E.; Takayama, S.; Jiang, X.; Ingber, D. E. *Annu. Rev. Biomed. Eng.* **2001**, *3*, 335−373.
(13) Umbanhowar, P. B.; Prasad, V.; Weitz, D. A. *Langmuir* **2000**, *16*, 347−351.
(14) Rezaei, M.; Radfar, P.; Winter, M.; McClements, L.; Thierry, B.; Warkiani, M. E. *Anal. Chem.* **2021**, *93*, 4584−4592.
(15) Berggren, W. T.; Westphall, M. S.; Smith, L. M. *Anal. Chem.* **2002**, *74*, 3443−3448.
(16) Zhang, W.; Li, N.; Koga, D.; Zhang, Y.; Zeng, H.; Nakajima, H.; Lin, J.-M.; Uchiyama, K. *Anal. Chem.* **2018**, *90*, 5329−5334.
(17) Maeda, K.; Onoe, H.; Takinoue, M.; Takeuchi, S. *Adv. Mater.* **2012**, *24*, 1340−1346.
(18) Chen, Z.; Liao, P.; Zhang, F.; Jiang, M.; Zhu, Y.; Huang, Y. *Lab Chip* **2017**, *17*, 235−240.
(19) Xu, P.; Zheng, X.; Tao, Y.; Du, W. *Anal. Chem.* **2016**, *88*, 3171−3177.
(20) Chen, Z.; Fu, Y.; Zhang, F.; Liu, L.; Zhang, N.; Zhou, D.; Yang, J.; Pang, Y.; Huang, Y. *Lab Chip* **2016**, *16*, 4512−4516.
(21) Mei, L.; Jin, M.; Xie, S.; Yan, Z.; Wang, X.; Zhou, G.; van den Berg, A.; Shui, L. *Lab Chip* **2018**, *18*, 2806−2815.
(22) Tang, S.-Y.; Wang, K.; Fan, K.; Feng, Z.; Zhang, Y.; Zhao, Q.; Yun, G.; Yuan, D.; Jiang, L.; Li, M.; Li, W. *Anal. Chem.* **2019**, *91*, 3725−3732.
(23) Li, H.-T.; Wang, H.-F.; Wang, Y.; Pan, J.; Fang, Q. *Talanta* **2020**, *217*, 120997.
(24) Hu, Y.; Xu, P.; Luo, J.; He, H.; Du, W. *Anal. Chem.* **2017**, *89*, 745−750.
(25) Tao, Y.; Yun, J.; Wang, J.; Xu, P.; Li, C.; Liu, H.; Lan, Y.; Pan, J.; Du, W. *Food Chem.* **2020**, *327*, 126945.
(26) Liao, S.; Tao, Y.; Du, W.; Wang, Y. *Langmuir* **2018**, *34*, 11655−11666.
(27) Liao, S.; Tao, X.; Ju, Y.; Feng, J.; Du, W.; Wang, Y. *ACS Appl. Mater. Interfaces* **2017**, *9*, 43545−43552.
(28) Kreutz, J. E.; Munson, T.; Huynh, T.; Shen, F.; Du, W.; Ismagilov, R. F. *Anal. Chem.* **2011**, *83*, 8158−8168.
(29) Blome, S.; Franzke, K.; Beer, M. *Virus Res.* **2020**, *287*, 198099.
(30) Majumdar, N.; Wessel, T.; Marks, J. *PLoS One* **2015**, *10*, No. e118833.

Supporting Information
OsciDrop: A Versatile Deterministic Droplet Generator

Shun Ye[1#†], Caiming Li[1,8#], Xu Zheng[2,*], Weihang Huang[5], Yi Tao[1], Yanghuan Yu[1], Limin Yang[6], Ying Lan[1], Liang Ma[3*], Shengtai Bian[4,*] and Wenbin Du[1,7,8,*]

[1] State Key Laboratory of Microbial Resources, Institute of Microbiology, Chinese Academy of Sciences, Beijing 100101, China

[2] State Key Laboratory of Nonlinear Mechanics, Institute of Mechanics, Chinese Academy of Sciences, Beijing 100190, China

[3] Dawei Biotechnologies Co., Ltd., Beijing 100085, China

[4] School of Sport Science, Beijing Sport University, Beijing 100084, China

[5] Department of Linguistics and Modern Languages, The Chinese University of Hong Kong, Hong Kong SAR, China

[6] CAS Key Laboratory of Pathogenic Microbiology and Immunology, Institute of Microbiology, Chinese Academy of Sciences, Beijing 100101, China

[7] Savaid Medical School, University of the Chinese Academy of Sciences, Beijing 100049, China

[8] College of Life Sciences, University of the Chinese Academy of Sciences, Beijing 100049, China

[#] These authors contributed equally to this work.

[†] Present address: Biomedical Engineering Department, College of Engineering, Pennsylvania State University, University Park, PA 16802, USA

* Correspondence: zhengxu@lnm.imech.ac.cn (X.Z.), liangma.chem@gmail.com (L.M.), stbian@bsu.edu.cn (S.B.), wenbin@im.ac.cn (W.D.)

Table of Contents

Text S1. The physical principles of OsciDrop

1. Detailed version of theoretical analysis of droplet segmentation by OsciDrop

To understand the droplet segmentation mechanism of the OsciDrop system, we develop a theoretical model based on the force balance of the droplet. The oscillation of the current OsciDrop system is along the horizontal direction. When the aqueous phase is flowing out of the micropipette tip, the growing droplet will be distorted by the horizontal shear flow of the oil phase. During the droplet segmentation, the droplet lags behind the oscillating tip due to the viscous drag of the oil phase, forming a horizontal "neck" of the aqueous stream (Fig. 2A). The dynamic forces exerting on the droplet during droplet segmentation include: the interfacial tension F_σ, the viscous drag force F_v, the inertial force F_i originated from the acceleration/deceleration of the tip oscillation, the gravity/buoyancy of the droplet, the kinetic force owing to the flow rate of the aqueous phase, and the lift force due to the pressure difference of the shear flow of the oil phase. The vertical forces like gravity/buoyance are neglected as the droplet segmentation by OsciDrop occurs in the horizontal direction. The kinetic force is also ignored in our analysis because it is much smaller than the interfacial tension F_σ and the viscous drag force F_v. We emphasize that the viscous drag force from the oil phase and the inertial force originating from the tip oscillation are two major effects causing the droplet segmentation when they exceed the interfacial tension at the neck. Based on the force balance $F_i + F_v = F_\sigma$, we deduce a final equation to describe the relationship among the aqueous phase injection speed u_f, the oscillation speed u, and the generated droplet radius R:

$$We\frac{u_f}{u}R + 6Ca(1-\frac{u_f}{u})R = d_{neck} \quad [S1]$$

Where We and Ca are the Webber number and capillary number, respectively, and d_{neck} is the characteristic dimension of the neck region. The We number, $We = \frac{\rho R_{tube}^2 uTa}{\sigma R}$, is the ratio between the inertial force and the interfacial tension, while the capillary number Ca, $Ca = \frac{\eta u}{\sigma}$, defines the ratio between the viscous force and the interfacial tension, where R_{tube} is the tube radius in the tip, ρ, σ, and η are the fluid density, the tension of the aqueous/oil interface, and the oil viscosity, respectively, and T and a are the period and acceleration of the oscillation. These two dimensionless numbers unveil that the droplet segmentation falls in two regions determined by either We-dominated or Ca-dominated mechanisms. The previous design of spinning emulsion generator works in the Ca-dominated range, in which the force balance is simplified as $F_v = F_\sigma$. In contrast, in the current OsciDrop system where accelerated/decelerated oscillation introduces the inertial force F_i, the droplet segmentation is dominated by the We number instead. In our experiments, the We number (~O(10)) is almost two orders of magnitude larger than the Ca number (~O(0.5)), indicating the significant contribution of the oscillation inertial force F_i.

We find that the OsciDrop system can precisely determine the moment when droplet segmentation occurs by adjusting the waveform of the oscillation and varying the inertial force F_i. We design the asymmetrical oscillation waveform by combining a long triangle wave (called the initial stage that lasts the first $4T/5$ in each period) plus a short cosinusoidal wave (called the segmenting stage that lasts the remaining $T/5$ in a period) (Fig. S2). We will show that this oscillation effectively achieved deterministic droplet segmentation with highly uniform droplet sizes in every single oscillation period. We calculate the temporal force variation under such asymmetrical oscillation (Fig. 2F, with oscillation frequency f = 120 Hz and 30 Hz). Thus, we can estimate when the summation of the inertial force F_i and the viscous drag force F_v exceeds the interfacial tension F_σ. In Fig. 2F, the interfacial tension F_σ is shown by the gray horizontal plane as it is independent of flow rate Q and elapsed time t, whereas the colored curved surface represents the summation of the breaking

force $F_i + F_v$. The droplet segmentation occurs in the segmenting stage $t > 4T/5$ when the colored surface $F_i + F_v$ is higher than the gray plane F_σ. When the oscillation frequency $f = 120$ Hz, the breaking force $F_i + F_v$ could be one order of magnitude larger than the interfacial tension, indicating a deterministic effect for droplet segmentation. While if the frequency is reduced to 30 Hz, the breaking force is only slightly larger than F_σ. We emphasize that there are a lower threshold flow rate $Q_{th\text{-}L}$ and an upper threshold flow rate $Q_{th\text{-}U}$, as being highlighted by the dashed lines in Fig. 2F, between which we generate perfectly monodisperse droplets. Thus, based on the theoretical analysis, we define three working ranges for the OsciDrop system: (1) Below $Q_{th\text{-}L}$, droplet segmentation cannot complete in one period as interfacial tension is dominant. (2) Between $Q_{th\text{-}L}$ and $Q_{th\text{-}U}$, the breaking force overcomes interfacial tension in a narrow region of the segmenting stage, forming the monodisperse range. (3) Beyond $Q_{th\text{-}U}$, the working range turns to polydisperse as the breaking force, and the interfacial tension becomes comparable even in the initial stage. We may obtain chaotic droplet segmentation or satellite droplet in the polydisperse range. We plot a phase diagram based on three working ranges to conclude the proper working condition (Fig. 2E).

2. Feasibility of generating droplets using different oscillation waveforms

Based on theoretical assumptions, we examine the feasibility of generating monodisperse droplets using different oscillation waveforms, including sine, square, and triangle waves. Part of the results is shown in Fig. S1. We find that it is challenging to generate monodisperse droplets in each period using symmetrical oscillation. Generally, for these symmetrical oscillations, the F_i value is relatively small under the small oscillating amplitude or oscillating frequency and has difficulty in overcoming the interfacial tension. While the oscillating amplitude and frequency are increased, the F_i may exceed the interfacial tension twice during one oscillating period, leading to poor monodispersity and difficulty in controlling the time point of segmentation. We briefly explain the shortcomings of these symmetrical oscillations. For instance, for sinusoidal oscillation, the inertial force F_i is usually smaller than that of an asymmetrical oscillation, which causes difficulty in generating uniform droplets with small volumes. Suppose we increase oscillation amplitude or frequency to overcome this problem. In that case, we will see nonuniform droplet segmentation happening twice in one oscillation period as the sinusoidal wave has two chances of reaching the maximum acceleration a in each period. For the square wave, inertial force F_i only exists during the instant switch from positive position to negative one, and *vice versa*. Theoretically, at this moment, the acceleration a and the inertial force F_i are both infinite, whereas a and F_i are quite large but dependent on the oscillator's property in practice. This causes chaotic droplet segmentation and undesired polydispersity. The square wave also leads to nonuniform droplet segmentation happening twice in one oscillation period as it has two instant switches in one period. For similar reasons, the triangle wave is not a suitable choice too. Thus, we propose an asymmetrical oscillation, consisting of an extended initial growth stage and a short segmenting stage, which would generate monodisperse droplets in a controllable manner. Results show that our asymmetrical waveform exhibits excellent performance for generating monodisperse droplets (Fig. S1).

3. Deduction of the force balance equation

During droplet segmentation in the OsciDrop system, there are following forces exerting on the droplet: the interfacial tension F_σ, the viscous drag force F_v, the inertial force F_i originated from the acceleration/deceleration of the tip oscillation, the gravity/buoyancy of the droplet, the kinetic force owing to the flow rate of the aqueous phase, and the lift force due to the pressure difference of the shear flow of the oil phase. The droplet segmentation of the OsciDrop system occurs under the horizontal oscillation, so the forces in the vertical direction are neglected. Considering that the droplet is spherical, the three horizontal forces thus

establish the force balance:

$$F_i + F_v = F_\sigma \quad [S2]$$

Where the forces on the left-hand side of Equation S2 try to detach the droplet from the aqueous stream, while the interfacial tension on the right-hand side resists the break-off. When the breaking force $F_i + F_v$ exceeds F_σ, droplet segmentation occurs.

The inertial force can be expressed based on the acceleration a of the oscillation:

$$F_i = ma = \rho QTa = \rho\pi R_{tube}^2 u_f Ta \quad [S3]$$

Where m is the droplet mass, Q is the flow rate of the aqueous phase. The viscous drag force F_v from the oil phase can be described based on the theory of the Stokes drag force:

$$F_v = 6\pi\eta R(u - u_f) \quad [S4]$$

The interfacial tension is exerted at the neck region, which is written as:

$$F_\sigma = \pi\sigma d_{neck} \quad [S5]$$

Substituting Equations S3 – S5 into Equation S2, we obtain:

$$\rho\pi R_{tube}^2 u_f Ta + 6\pi\eta R(u - u_f) = \pi\sigma d_{neck} \quad [S6]$$

Both sides of Equation S6 are divided by $\pi\sigma$, and we deduce the final equation (Equation 1 in the paper) by defining the *We* number and the capillary number:

$$We\frac{u_f}{u}R + 6Ca(1 - \frac{u_f}{u})R = d_{neck} \quad [S7]$$

The *We* number and *Ca* number unveil two different ranges of the droplet segmentation, respectively: inertial force-dominated range and viscous force-dominated range.

4. Novel *We*-dominated mechanism different from previously *Ca*-dominated mechanism

We stress that the mechanism of our OsciDrop system is totally different from the previous spinning/revolving droplet generator [1-2]. Herein, we clarify their mechanisms by quantifying the dimensionless *We* and *Ca* numbers based on Equation S7. For spinning/revolving droplet generator, as the uniform circular motion of the droplet doesn't introduce the inertial force, the *We* number is zero, and the droplet segmentation is only determined by the *Ca* number, indicating a viscous force-dominated mechanism. Thus, in *Ca*-dominated regime, Equation S7 can be simplified as:

$$R = \frac{d_{neck}}{6Ca(1 - {}^{u_f}/_u)} \quad [S8]$$

Which is similar to the theoretical result in ref [1]. The reported spinning speed is more than 1000 rpm, corresponding to a *Ca* number in the range of 1 - 5.

However, in the OsciDrop system, the inertial term governed by the *We* number becomes dominated. Based on the definition of the *We* and *Ca* numbers, we calculated their values to compare their effects. In the calculation, the values of all parameters are the same as those used in our experiments, which are listed below. The interfacial tension is σ =0.008 N/m, the oil phase viscosity and density (collected by Lovis 2000 M/ME, Anton Paar Shanghai Trading Co., Ltd.) are η = 0.025 Pa·s and ρ = 0.86 g/cm^3 respectively, the tube radius of the micropipette tip is R_{tube} = 60 μm, the flow rate Q of the aqueous phase can be adjusted from approximately 10 nL/s to more than 1500 nL/s, the amplitude of the oscillation A is usually about 0.5 mm, and the oscillation frequency is set to 120 Hz. At last, there is one parameter, the neck diameter d_{neck}, the value of which is difficult to assign. According to the literature [3], d_{neck} was usually found to be d_{neck}=0.4R. We use this result in

the calculation. Thus, we obtain that the *We* number is *We* = 11.6, which is 23 times larger than the *Ca* number *Ca* ~ 0.5. The large *We* number clearly manifests the inertial force-dominated mechanism, while the viscous effect is not sufficient to complete droplet segmentation as *Ca* < 1. More importantly, the *We* number in the OsciDrop system is even larger than the *Ca* number in the spinning/revolving system, indicating a stronger segmenting effect from the inertial force. We conclude that this inertial force is the key mechanism for droplet generation with OsciDrop.

Furthermore, we stress that the *We*-dominated mechanism of the OsciDrop method shows high compatibility with the continuous phase of different viscosities, as the *We* regime is not sensitive to the change of the oil viscosity with a small *Ca*. We have experimentally verified that the *We*-dominated mechanism of the OsciDrop method can work perfectly in other oil phases with different viscosities, even in fluorinated oil with higher density (More details are provided in Text S3 and Fig. S6). For the fluorinated oil, the interfacial tension is σ = 0.0048 N/m, and the oil phase viscosity and density (Droplet Generation Oil for Probes, Bio-Rad, USA) are η = 0.0014 Pa.s and ρ = 1.62 g/cm^3, respectively. The *We* number becomes even higher, *We* = 36.8, compared with the small *Ca* ~ 0.05.

5. Force analysis for the asymmetrical oscillation

We establish an asymmetrical oscillation (see Fig. S2) by combining a long triangle wave (which lasts the first 4*T*/5 in each period) with a short cosinusoidal wave (which lasts the remaining *T*/5 in each period) in a period. We find that this asymmetrical oscillation is more efficient in achieving highly uniform droplet segmentation during each oscillation period. In such a configuration, the inertial force F_i can be divided into two parts: when $0 < t < 4T/5$ (called the initial stage), $F_i = 0$ as the droplet displacement varies linearly with time t and the acceleration equals zero. When $4T/5 < t < T$ (called the segmenting stage), for a cosinusoidal wave with displacement $x(t)=-A\cos[5\pi(t-4T/5)/T]$, the acceleration $a(t)$ can be calculated by taking the derivative twice:

$$a(t) = A(\frac{5\pi}{T})^2 cos[\frac{5\pi}{T}(t - \frac{4}{5}T)] \quad [S9]$$

Thus, the inertial force can be deduced as:

$$F_i = \rho\pi R_{tube}^2 u_f t A(\frac{5\pi}{T})^2 cos[\frac{5\pi}{T}(t - \frac{4}{5}T)] \quad [S10]$$

As a result, we obtain Equation 4 in the *Results* section to describe the inertial force. The viscous drag force and the interfacial tension are still described by Equations S5 and S6, respectively.

We find that the triangle wave can serve as a "force switch" as its linear motion results in zero inertial force, and the cosinusoidal waves can be used to precisely determine the moment when the maximum inertial force should be applied. The reason is that at the turning moment $t = 4T/5$ the inertial force suddenly reaches its maximum value, according to Equation S10. This maximum inertial force F_i at the turning moment results in a sharp increase of the breaking force $F_i + F_v$ at the same moment. Therefore, we can precisely design when the segmenting occurs based on the turning moment connecting with a cosinusoidal wave. We will employ the force plot explained below to highlight the turning moment and different working ranges. In addition, extending the length of the initial stage and reducing the length of the segmenting stage can also increase the inertial force F_i.

6. Force plot and three working ranges

Based on Equations S4, S5, and S10, we calculated the temporal variation of the major forces in one oscillation period. Thus, a three-dimensional (3D) force plot among the interfacial tension F_σ, the viscous drag force F_v, and the inertial force F_i can be provided to compare different effects. The force plots of the asymmetrical oscillation used in the current experiments have been shown in Fig. 2F. The *x* and *y* axes in the

3D plot are the elapsed time t (ms) and the flow rate Q (nL/s), and the vertical z axis indicates the values of different forces. The interfacial tension F_σ that resists droplet segmentation is displayed by the gray surface. According to Equation S4, the interfacial tension F_σ is constant and independent of t and Q. The summation of the F_i and F_v that causes droplet break-off is shown by the colored curved surface, in which red means larger force and blue means smaller force. The force comparison plot clearly shows that in one single period, there is a region where $F_i + F_v > F_\sigma$. The corresponding time t and flow rate Q in this region indicate the condition to achieve a successful droplet segmentation. As mentioned above, the sharp increase of the breaking force occurs just after the turning moment $t = 4T/5$, which is verified by the crossover of the colored surface ($F_i + F_v$) above the gray horizontal plane F_σ.

The force plot helps understand the existence of three working ranges of the OsciDrop system. As indicated by the dashed lines in Fig. 2F, a lower threshold flow rate $Q_{th\text{-}L}$ can be clearly seen, below which $F_i + F_v$ is always smaller than F_σ, and the droplet segmentation does not occur in this period. When the oscillation frequency $f = 120$ Hz, the lower threshold flow rate is found to be about $Q_{th\text{-}L} = 20$ - 30 nL/s. If the frequency is reduced to 30 Hz, the $Q_{th\text{-}L}$ will increase to about 150 nL/s, implying an increasing barrier to generate small droplets at a low flow rate. Note that when flow rate Q is large enough, there is another threshold $Q_{th\text{-}U}$. Above this upper threshold $Q_{th\text{-}U}$, the breaking force ($F_i + F_v$) dominating droplet segmentation and the interfacial tension become comparable even in the initial growth stage, resulting in nonuniform droplet segmentation or generation of satellite droplets. The upper threshold flow rate is about $Q_{th\text{-}U} = 1400$ nL/s when the oscillation frequency $f = 120$ Hz. Thus, we conclude the monodisperse range (within the two dashed lines in Fig. 2F) in between the two threshold flow rates $Q_{th\text{-}L}$ and $Q_{th\text{-}U}$.

Based on these two threshold flow rates, we summarize a phase diagram of the droplet segmentation as shown in Fig. 2E. The three different working ranges are clearly displayed in the phase diagram. The monodisperse range is in the middle, whereas in the left one with smaller amplitudes and flow rates, the droplet segmentation frequency is usually half of the oscillation frequency, and in the right one with larger amplitudes and flow rates, the droplet is also nonuniform and the droplet segmentation frequency is larger than the oscillation frequency. We provide a blue dashed line and a red dashed line in the phase diagram (Fig. 2E) to predict the boundaries between different working ranges theoretically. This theoretical prediction is numerically calculated based on the corresponding crossover point between $F_i + F_v$ and F_σ. We can see good agreement between the prediction and the experimental observation (experimental results of different working ranges are categorized by different symbols in Fig. 2E).

7. Performance of sinusoidal oscillation and corresponding force plot

We attempted to generate droplets using other oscillation waveforms. We successfully generated 1 nL to 12 nL droplets using sine waves (Fig. S5) by adjusting three control parameters.

We take sinusoidal oscillation as an example to show its force plot and compare it with asymmetrical oscillation. The displacement of a sinusoidal wave is $x(t) = A\sin(2\pi t/T)$, so the acceleration $a(t)$ can be calculated as:

$$a(t) = -A(\frac{2\pi}{T})^2 sin(\frac{2\pi}{T}t) \quad [S11]$$

And the inertial force is:

$$F_i = -\rho\pi R_{tube}^2 u_f t A(\frac{2\pi}{T})^2 sin(\frac{2\pi}{T}t) \quad [S12]$$

The negative signs in Equations S11 and S12 only determine the direction. The equation of the inertial force F_i under sinusoidal oscillation (Equation S12) is similar to that under asymmetrical oscillation given in

Equation S9, implying that sinusoidal oscillation could also work with proper flow rate and oscillation frequency/amplitude. As shown in Fig. S5A, we can obtain highly uniform droplets from about 2 - 5 nL under a 120 Hz sinusoidal oscillation. To generate 1 nL or smaller droplets uniformly, we have to increase the frequency to 160 Hz (corresponding to decrease T in Equation S12) to increase the inertial force F_i according to Equation S12. Compared with Equation S10, the F_i of sinusoidal oscillation is smaller than that of the asymmetric oscillation, owing to the prefactor $(2\pi)^2$ in Equation S12 instead of $(5\pi)^2$ in Equation S10. We show the force plot under 120 Hz sinusoidal oscillation using a low flow rate in the left of Fig. S5B. We can see that the lower threshold flow rate $Q_{th\text{-}L}$ is about 180 nL/s, below which the breaking force is not large enough to overcome interfacial tension. According to Equation 3, this lower threshold $Q_{th\text{-}L}$ means that the smallest droplet that can be obtained under 120 Hz oscillation is about 180/120 = 1.5 nL. If we further increase the flow rate to be more than 1000 nL/s, we can see from Fig. S5A that droplet segmentation is achieved twice in one oscillation period. To explain this phenomenon, we calculate the temporal variation of the breaking force. In the calculation, if the droplet segmentation is completed when the breaking force exceeds the interfacial tension, the elapsed time t in Equation S12 will be reset to zero to simulate the start of another droplet segmentation. The force plot for large flow rates is shown in the right of Fig. S5C, in which we can see two similar peaks of the breaking force in both halves of the oscillation period. The force plot predicts that we will obtain double droplet segmentation in one oscillation period when the flow rate is larger than approximately 1200 nL/s. The prediction is consistent with the experimental observation shown in Fig. S5A. However, droplet generation by sinusoidal oscillation was more susceptible to tip geometry, resulting in larger variations.

Text S2. Droplet generation using the standard 10-μL micropipette tip

In addition to the generation of monodisperse droplets using customized micropipette tips with an i.d. of 100~150 μm, we also successfully generated monodisperse nanoliter droplets using the standard 10 μL micropipette tip with an i.d. 400 μm. Due to the relatively large inner diameter of the orifice, the surface tension is dominant at the beginning (called pre-initial stage). This pre-initial stage lasted until the aqueous phase protruded into the oil phase and reached equilibrium. Then, the droplet segmentation process became similar to that of customized micropipette tips mentioned before, which contained two stages in a repeatable period: During a long initial stage, the aqueous stream bulged and elongated in the oil phase and was segmented into monodisperse droplets during a short segmenting stage. The droplet generation process is schematically illustrated in Fig. S3 and the results are shown in Fig. 3G and 3H. Successful generation of monodisperse 1-nL and 12-nL droplets using standard 10 μL micropipette tip provides a good example to demonstrate the robustness of the OsciDrop system.

Text S3. Additional validations of OsciDrop.

In addition, we tested if we could further expand the dynamic range of droplet generation volume by OsciDrop. As a result, we generated 10 pL and 100 pL droplets successfully using a high-precision infusion pump (PHD Ultra, Harvard Apparatus, USA) (Fig. S4) by reducing the Q_c value.

We also validated the feasibility of using denser fluorinated oil (Droplet Generation Oil for Probes, Bio-Rad, USA) as the continuous phase to generate uniform w/o droplets (Fig. S6). The working mechanism was still based on the high inertial effect indicated by the *We* number. As estimated in Text S1.4, the *We* number changed to 36.8 when high-density fluorinated oil was used, three orders of magnitudes larger than the *Ca* number of 0.05. Although the fluorinated oil density is higher than water, the droplet generation of the OsciDrop was based on the force balance along the horizontal oscillation direction, which could be explained

by the same theoretical model when hydrocarbon oil was used. We experimentally obtained 1 nL droplets using denser fluorinated oil (Fig. S6). We observed that the droplets were intact, and the oscillating tip did not affect the integrity of droplets (Movie S4).

To test if the chip-based approach allows a similar "mix-and-match" type of operation with reagents under default experimental setup, we used the QX-200 droplet generator and DG8™ Cartridges (Bio-rad, USA) as a control to generate droplets with different reagents and continuous phases (Fig. S7). We found that the hydrocarbon oil cannot flow into DG8™ Cartridges, presumably due to the high viscosity and swelling or even dissolution of microchannels by hydrocarbon oil, and failed to generate droplets. On the other hand, droplet generation using fluorinated oil and hydrocarbon oil were both achieved by OsciDrop.

Supporting References:

1. Chen, Z.; Fu, Y.; Zhang, F.; Liu, L.; Zhang, N.; Zhou, D.; Yang, J.; Pang, Y.; Huang, Y. *Lab Chip* **2016**, *16* (23), 4512-4516.
2. Zhang, Y.; Zhao, Q.; Yuan, D.; Liu, H.; Yun, G.; Lu, H.; Li, M.; Guo, J.; Li, W.; Tang, S.-Y. *Lab Chip* **2020**, *20* (24), 4592-4599.
3. Zhang, X. G.; Basaran, O. *Phys. Fluids* **1995**, 7,1184.
4. Tjahjadi, M.; Stone, H. A.; Ottino, J. M. *J. Fluid Mech.* **1992**, 243, 297-317.

Supporting Tables

Table S1. Primers for African swine fever virus (ASFV) detection with dLAMP.

Primer	Oligonucleotide sequence
FIP	5'-GCCTCGTTGGTGGAAAGGATCCTTCAACGCATAGGAGAC-3'
BIP	5'-TGGCGGGAGAGGAAGGAACTATGACGGCGTAATGAAGAT-3'
F3	5'-GCATGTACTACAACGATTAGGA-3'
B3	5'-AAGTCGCCGATTTGGTTT-3'

Table S2. A set of primers and a probe for EIF5B gene detection with MV digital PCR.

Primer/Probe	Oligonucleotide sequence
EIF5B-F	5'-ATGAGATGCCAAACTTCAGC-3'
EIF5B-R	5'-GGCAACATTTCACACTACAG-3'
EIF5B-P	VIC-CTCTTCTCATGCAGTTGTCAGAAG-MGB

Table S3. The numbers of droplets per well and experimental replicates for MV-dPCR.

Droplet voume (nL)	Number of droples per well	Repeats and Number of wells
0.2	14100	3 reps × 4 wells
0.5	7800	3 reps × 4 wells
1	4750	3 reps × 4 wells
2.5	2400	3 reps × 4 wells
5	1600	3 reps × 4 wells

Table S4. Three primary control parameters (Q, A, f) for generating monodisperse droplets spanning picoliter to microliter range.

Expected droplet volume V	Flow rate Q	Oscillating frequency f	Oscillating amplitude A
200 pL	24 nL/s	120 Hz	0.77 mm
500 pL	60 nL/s	120 Hz	0.75 mm
1 nL	120 nL/s	120 Hz	0.55 mm
5 nL	500 nL/s	100 Hz	0.54 mm
10 nL	1000 nL/s	100 Hz	0.47 mm
50 nL	1000 nL/s	20 Hz	0.75 mm
100 nL	500 nL/s	5 Hz	1.14 mm
500 nL	500 nL/s	1 Hz	1.14 mm
1 μL	500 nL/s	0.5 Hz	1.14 mm
2 μL	1000 nL/s	0.5 Hz	1.14 mm

Table S5. The upper limit of quantification (ULQ), lower detection limit (LDL), and Errors of MV-dPCR.

Partition Volume (nL)	ULQ[1] (copies/μL)	ULQ Error (%)	LDL[2] (copies/μL)	LDL Error (%)
0.2	8.4×10^5	4.74	4×10^1	11.74
0.5	1.8×10^5	7.91	1.5×10^1	12.68
1	5.6×10^4	1.80	8×10^0	13.84
2.5	1.2×10^4	10.70	3.2×10^0	9.62
5	3.8×10^3	10.07	1.6×10^0	12.36

Multivolume	8.4×10^{5}	3.65	1.6×10^{0}	7.17

[1] The ULQ for each condition is the observed concentrations when the fraction of positive droplets is 0.95. [2] The LDL for each condition is that there are five positive partitions in one reaction.

Supporting Figures:

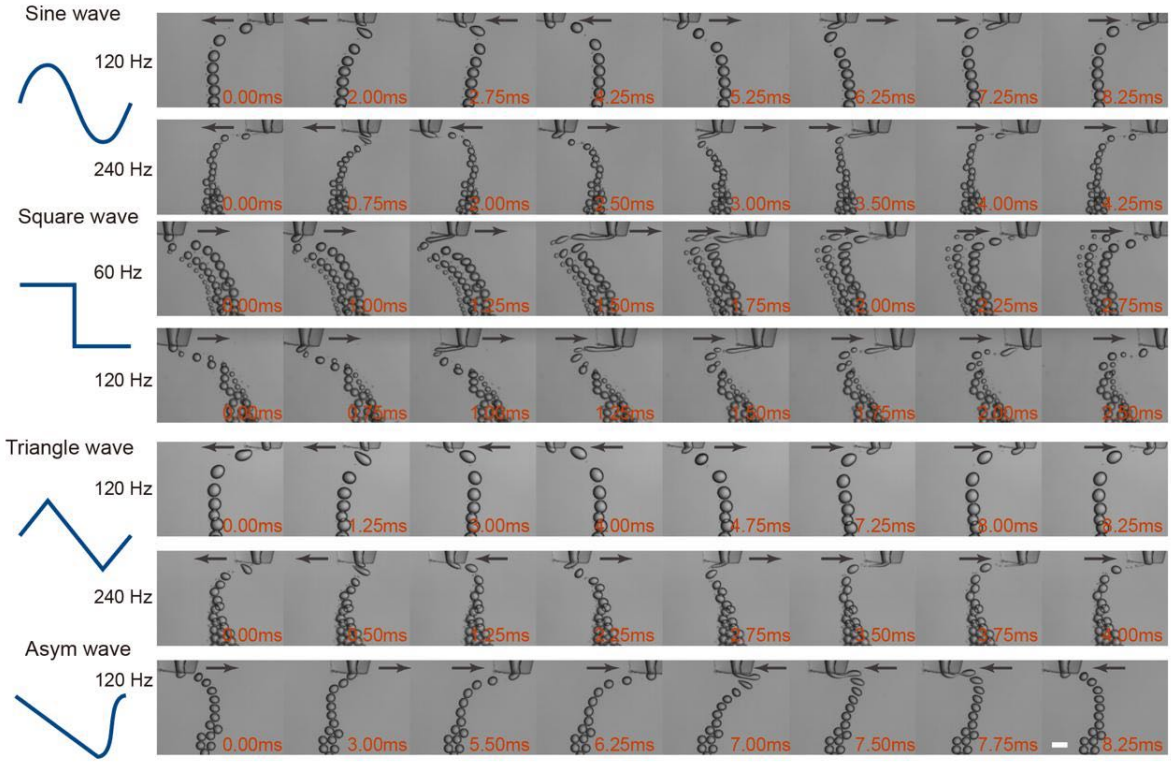

Fig. S1 Droplet generation using different oscillation waveforms, including sine, square, triangle, and asymmetrical waves. The scale bar is 200 μm.

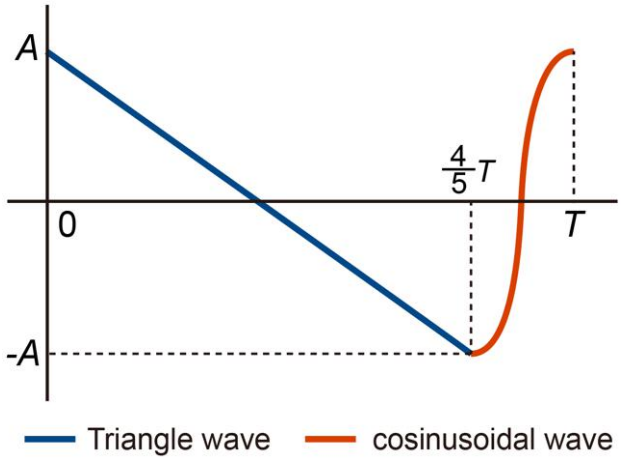

Fig. S2 Each period of the asymmetrical oscillation waveform consists of a long triangle wave (called initial stage) that lasts the first 4*T*/5 and a short cosinusoidal wave (called segmenting stage) that lasts the remaining *T*/5.

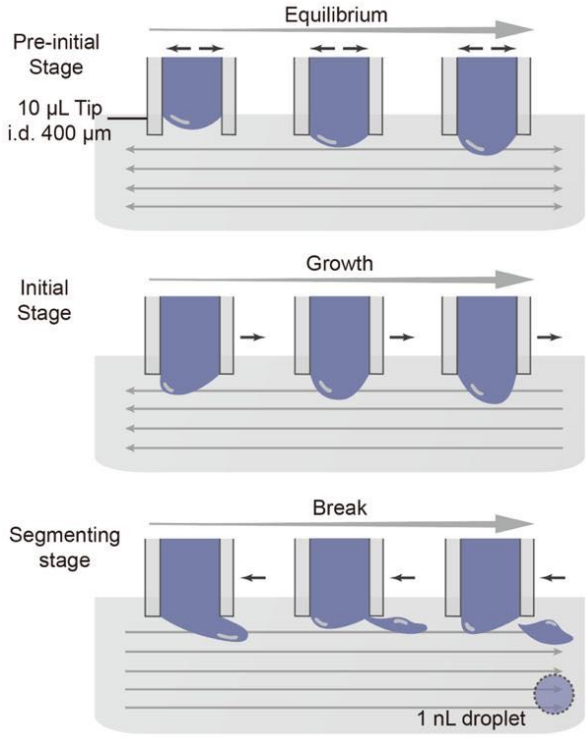

Fig. S3 A schematic illustration of the working principle and a droplet generation cycle using the standard 10-µL micropipette tip. The droplet generation process includes a pre-initial stage that the head of the aqueous stream cannot be segmented into droplets as surface tension is dominant. After the pre-initial stage, the droplet segmentation begins. During a long initial stage, the aqueous stream bulges and elongates in the oil phase and is segmented into monodisperse droplets during a short segmenting stage. Black arrows indicate the moving direction of the micropipette tips. Gray arrows represent the direction of relative motion of the oil phase.

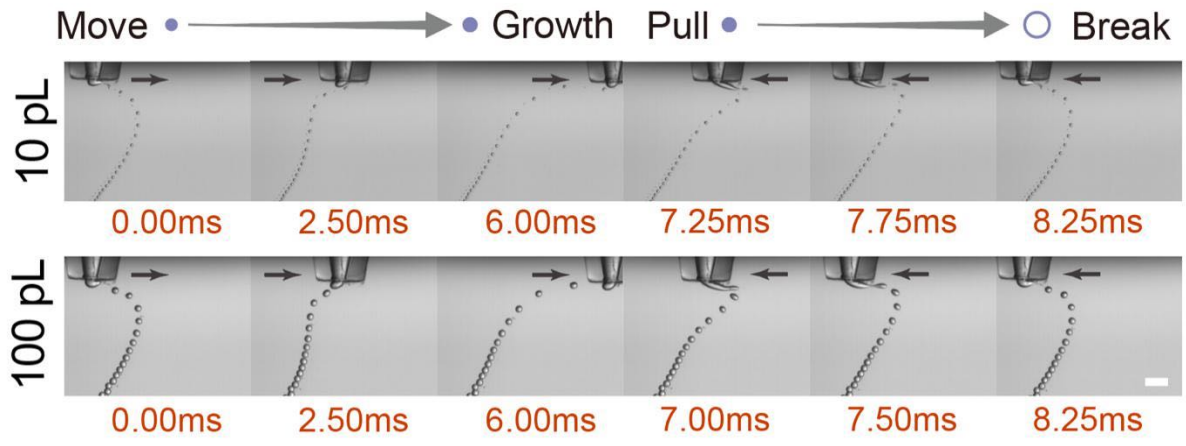

Fig. S4 Time-series microscopic images of the droplet generation cycle with expected volumes of 10 pL and 100 pL under 120 Hz asymmetrical oscillation. Black arrows indicate the moving direction of the micropipette tip. The scale bar is 200 µm.

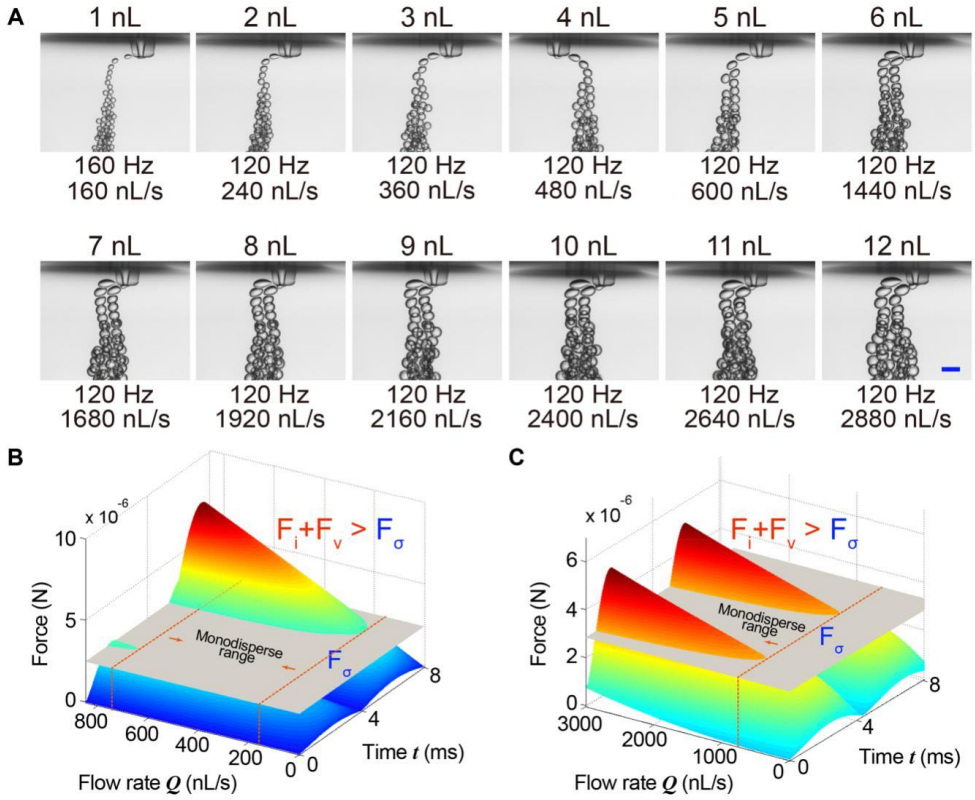

Fig. S5 Droplet generation under sinusoidal oscillation with OsciDrop. (A) Size-tunable generation of monodisperse nanoliter droplets from 1 nL to 12 nL. The scale bar is 400 μm. (B and C) Theoretical force comparison three-dimensional (3D) maps showing the temporal variations of $F_i + F_v$ (colorful curved surface) and F_σ (gray surface) under 120 Hz sinusoidal oscillation during one period T at low flow rates (B) and high flow rates (C).

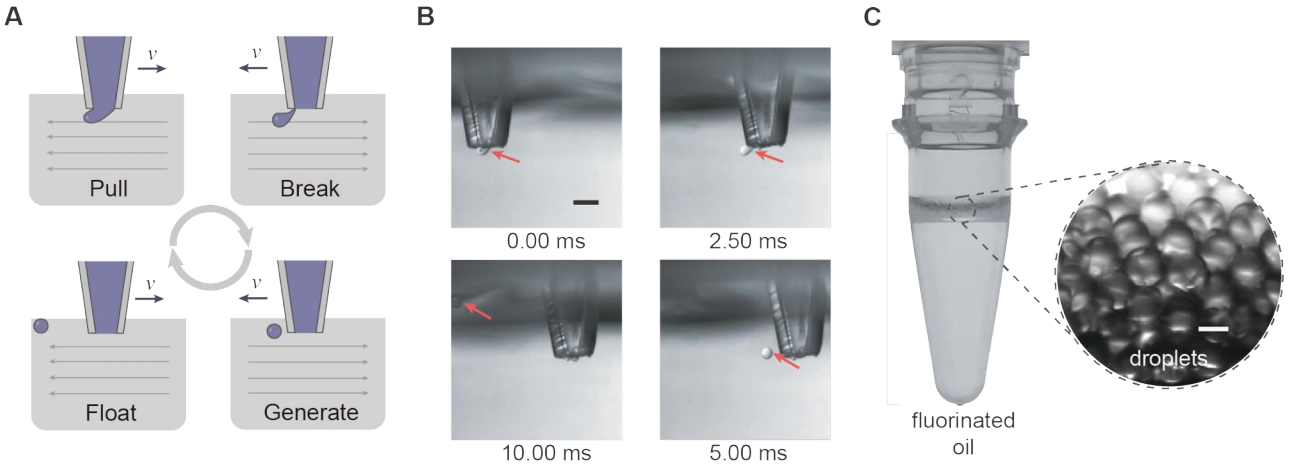

Fig. S6 Droplet generation using fluorinated oil. (A) Schemetics and (B) time-series images captured by the high-speed camera of a droplet generation cycle. The continuous phase is fluorinated oil. The scale bar is 300 μm. (C) The generated droplet cluster in the oil surface within the PCR tube. A magnified view shows monodisperse droplets. The scale bar is 100 μm.

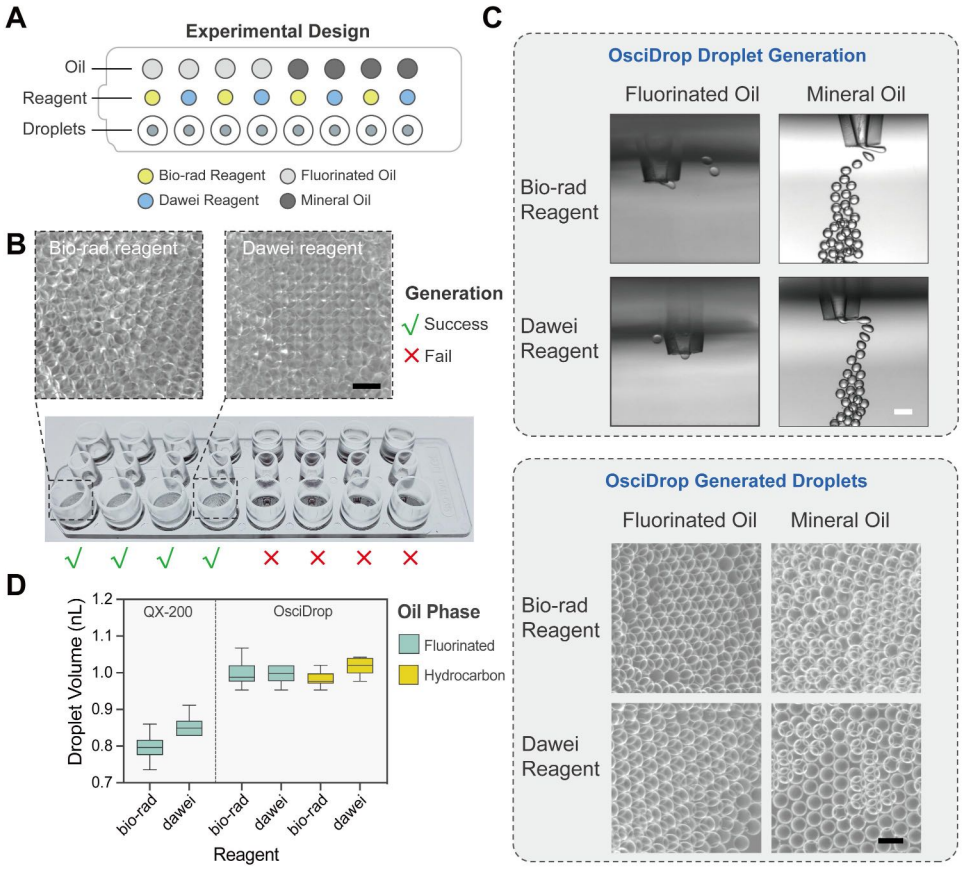

Fig. S7 Comparison of droplet generation by QX-200 (Bio-Rad) and OsciDrop. (A) Experimental design of droplet generation using QX-200. (B) Photo of DG8™ Cartridges after droplet generation and microscopic images of generated droplets. (C) Optical images of the droplet generation process and generated droplets, the scale bar is 200 μm. (D) The volume of generated droplets is measured with a CV of less than 5%.

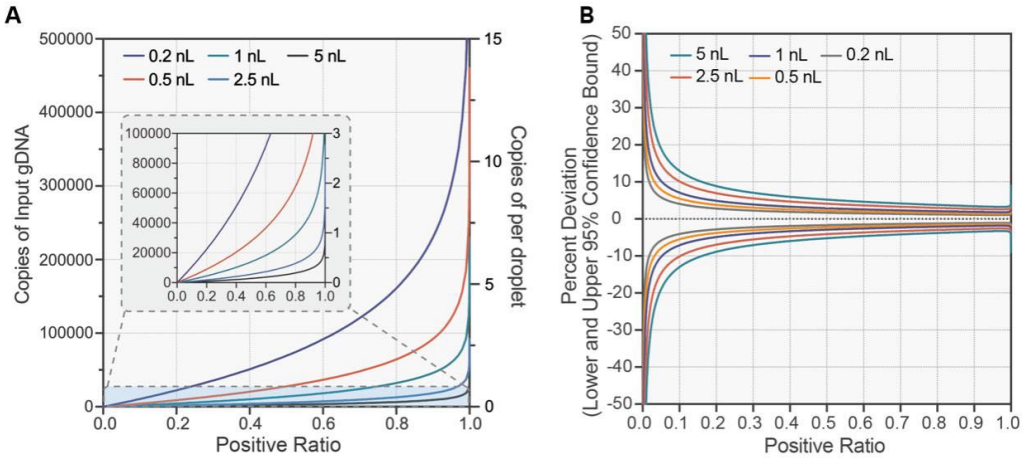

Fig. S8 Quantification range and precision of Multivolume digital PCR (MV-dPCR). (A) Theoretical calculation of the upper limit of quantification of copies based on Poisson distribution. 20 μL reaction was used as a demonstration, the partition volumes were set as 0.2 nL, 0.5 nL, 1 nL, 2.5 nL, and 5 nL. The partition volumes decrease with the increasing number of partitions and higher upper limit of quantification (ULQ). (B) Estimated confidence intervals for a variety of partition volumes.